Inorganic Chemistry

Article

pubs.acs.org/IC

Visible and Near-Infrared Emission from Lanthanoid β-Triketonate Assemblies Incorporating Cesium Cations

Laura Abad Galán,[†] Brodie L. Reid,[†] Stefano Stagni,[‡] Alexandre N. Sobolev,[§] Brian W. Skelton,[§] Massimo Cocchi,[∥] Joanna M. Malicka,[∥,¶] Eli Zysman-Colman,[*,⊥] Evan G. Moore,[*,#] Mark I. Ogden,[*,†] and Massimiliano Massi[*,†]

[†]Department of Chemistry and Curtin Institute of Functional Molecules and Interfaces, Curtin University, Kent Street, Bentley 6102, Western Australia, Australia

[‡]Department of Industrial Chemistry "Toso Montanari", University of Bologna, viale del Risorgimento 4, Bologna 40136, Italy

[§]School of Molecular Sciences, University of Western Australia, 35 Stirling Highway, Crawley, Perth, Western Australia 6009, Australia

[∥]Institute for Organic Synthesis and Photoreactivity (ISOF), Consiglio Nazionale delle Ricerche (CNR), Via P. Gobetti 101, 40129 Bologna, Italy

[⊥]Organic Semiconductor Centre, EaStCHEM School of Chemistry, University of St. Andrews, St. Andrews, Fife KY16 9ST, United Kingdom

[#]School of Chemistry and Molecular Biosciences, University of Queensland, St Lucia, Queensland 4072, Australia

Supporting Information

ABSTRACT: The reaction of the β-triketonate ligands tris(4-methylbenzoyl)methanide and tribenzoylmethanide with the trivalent lanthanoids Eu^{3+}, Er^{3+}, and Yb^{3+} in the presence of Cs^+ afforded polymeric structures where the repeating units are represented by bimetallic tetranuclear assemblies of formulation $\{[Ln(Cs)(\beta\text{-triketonate})_4]_2\}_n$. The only exception is the structure formed by the reaction of tris(4-methylbenzoyl)-methanide, Yb^{3+}, and Cs^+, which yielded a polymeric assembly where the repeating units are mononuclear Yb^{3+} complexes bridged by Cs^+ cations. Photophysical measurements on the obtained materials confirmed efficient sensitization from the ligand excited states to the 4f* excited states of the three lanthanoids. According to transient absorption data, Er^{3+} and Yb^{3+} are sensitized via energy transfer from the triplet state of the β-triketonate ligands. On the other hand, energy transfer to Eu^{3+} seems to occur via an alternative pathway, possibly directly via the singlet state or through ligand to metal charge transfer states. The emission measurements confirm efficient sensitization for all three lanthanoids and bright near-infrared emission for Er^{3+} and Yb^{3+}, a characteristic that seems to be linked to the specific chemical structure of the β-triketonate ligands.

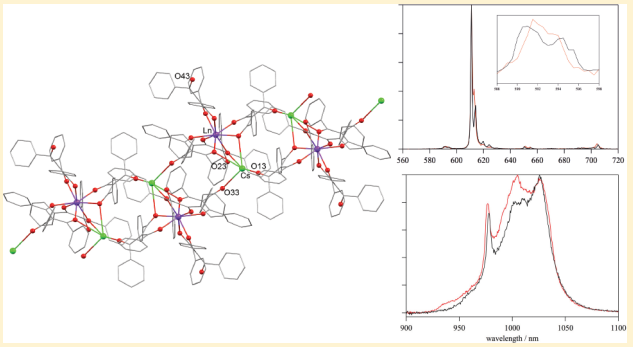

INTRODUCTION

The photophysical properties of trivalent lanthanoid cations are currently the focus of extensive investigation, stemming from their potential application in a variety of fields including optical displays, night vision devices, telecommunication signaling, life science, and counterfeiting technologies.[1−6] Lanthanoid cations cannot be directly excited in an efficient manner, a limitation that arises from f−f transitions being parity and often spin forbidden.[7−10] Therefore, efficiently luminescent lanthanoid complexes are obtained by exploiting sensitization through π-conjugated ligands. These ligands act as antennas by absorbing energy more efficiently and subsequently transferring this energy to populate the 4f* lanthanoid excited states. The general rules that govern efficient sensitization are well established and usually rely on the energy difference between the triplet excited state of the antenna - populated via intersystem crossing (ISC) from the singlet state and facilitated by the strong spin−orbit coupling of lanthanoid cations — and the accepting 4f* state.[11−13] However, it has been established that alternative pathways are also possible, such as direct sensitization from the ligand singlet excited state or energy transfer mediated by population of charge transfer states.[14−16] Another important consideration for the design of emissive lanthanoid complexes is the minimization of quenching via multiphonon relaxation, where the 4f* excited state transfers the energy to vibrational overtones of OH, NH, and CH bonds in close proximity to the lanthanoid cation.[11] This aspect is

Received: April 17, 2017
Published: July 11, 2017

DOI: 10.1021/acs.inorgchem.7b00928
Inorg. Chem. 2017, 56, 8975−8985

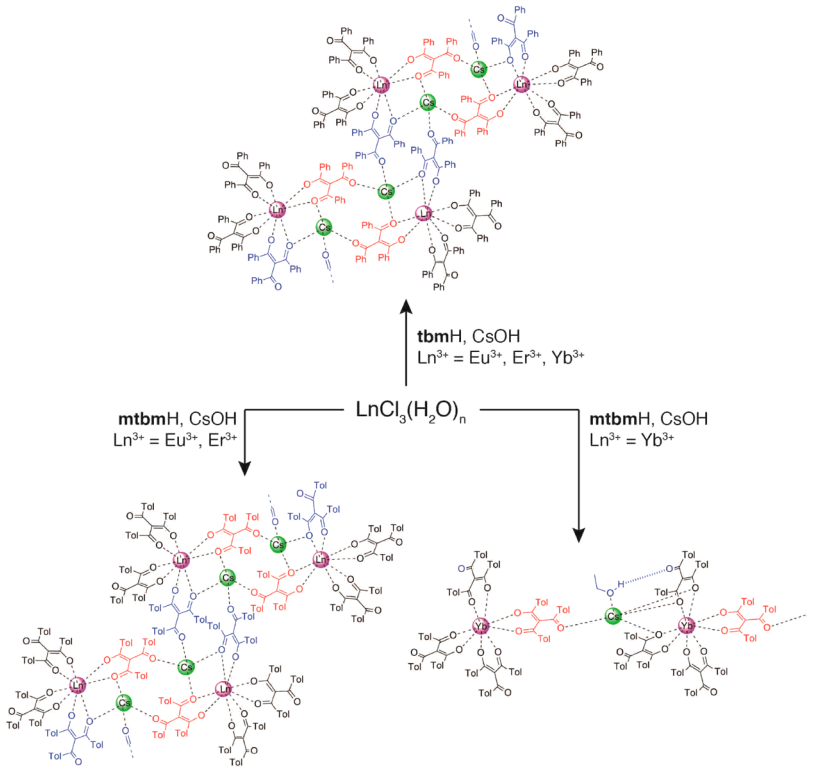

Figure 1. Summary of the isolated assemblies according to reaction conditions.

particularly important for those lanthanoid elements emitting near-infrared (NIR) radiation (e.g., Nd^{3+}, Er^{3+}, and Yb^{3+}), which are more susceptible than visible emitters (e.g., Eu^{3+} and Tb^{3+}) to these quenching phenomena.[17,18]

β-Diketonate ligands have been extensively investigated in lanthanoid coordination chemistry.[3,19] In fact, these types of ligands easily chelate the strongly oxophilic lanthanoid cations. Research in this domain has yielded a wide variety of structural motifs, ranging from mononuclear complexes to architecturally more sophisticated discrete oxo/hydroxo clusters.[20,21] Indeed, not only have β-diketonate ligands been useful in stabilizing a wide variety of structures but also their chemical composition can include aromatic moieties that favor the efficient sensitization of lanthanoid cations.[22−25]

In comparison to β-diketonates, β-triketonate ligands have been scarcely considered in lanthanoid coordination chemistry, with only a handful of examples being reported during the 1960s.[26−28] This lack of investigation is rather surprising, especially when one considers that these systems can be easily obtained by starting from ubiquitously available β-diketonates and well-established synthetic procedures based on Claisen-type condensation reactions. We have therefore endeavored to fill this gap and investigate the potential of β-triketonates for the synthesis of luminescent lanthanoid complexes. Our initial results highlighted the serendipitous discovery of discrete bimetallic tetranuclear assemblies of formulation $[Ln(Ae{\cdot}HOEt)(\mathbf{tbm})_4]_2$, where Ae^+ is an alkali-metal cation and $\mathbf{tbm}^-$ is the tribenzoylmethanide ligand.[29] Our studies have shown that this assembly is consistently obtained upon variation of the lanthanoid cation (Eu^{3+}, Er^+, and Yb^{3+}), alkali-metal cation (Na^+, K^+, or Rb^+), and alcoholic solvent (ethanol or *n*-butanol). Despite the structural novelty of these species, the most remarkable discovery occurred on investigating the photophysical properties of these lanthanoid assemblies. While the luminescent properties in the case of Eu^{3+} were similar to those of analogous complexes bound to diketonate ligands, exceptional NIR emission was recorded for assemblies of Er^{3+} and Yb^{3+}.[29] In particular, these assemblies exhibited remarkably elongated excited state lifetime decays, with values usually obtained from complexes bound to deuterated or fluorinated organic ligands designed to minimize quenching via multiphonon relaxation.[30] Furthermore, we demonstrated how these assemblies can be exploited as material precursors for the fabrication of near-infrared organic light emitting devices (NIR-OLEDs).[31]

In this work, we focus on completing the series, synthesizing lanthanoid assemblies incorporating Cs^+ as the alkali-element cation. Furthermore, we extend our investigation by using the new ligand tris(4-methylbenzoyl)methane (**mtbm**H) alongside the previously employed tribenzoylmethane (**tbm**H). Studying **mtbm**H is an initial step toward establishing how chemical modifications of the ligand might influence the specific structure of the species obtained. As in our previous studies, the resulting assemblies have been investigated by means of absorption and emission spectroscopy to characterize their photophysical properties. Additional transient absorption experiments have been conducted using simpler model complexes in an effort to further elucidate the detailed sensitization pathways that characterize lanthanoid species bound to β-triketonate ligands.

RESULTS AND DISCUSSION

Synthesis of the Lanthanoid Assemblies. The **mtbm**H ligand was synthesized following the same procedure previously reported for **tbm**H.[31] Following the same methodology used for the preparation of discrete tetranuclear $[Ln(Ae{\cdot}HOEt)(\mathbf{tbm})_4]_2$ (Ae^+ = Na^+, K^+, Rb^+) assemblies,[29] 1 equiv of hydrated $LnCl_3$ (Ln^{3+} = Eu^{3+}, Er^{3+}, Yb^{3+}) was made to react

DOI: 10.1021/acs.inorgchem.7b00928
Inorg. Chem. 2017, 56, 8975−8985

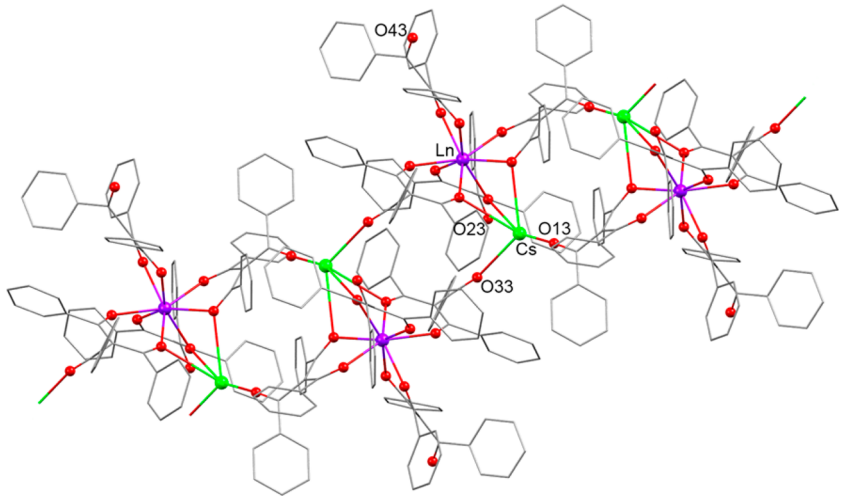

Figure 2. Representation of the X-ray crystal structure of $\{[Ln(Cs)(\mathbf{tbm})_4]_2\}_n$ (Ln^{3+}= Eu^{3+}, Er^{3+}, Yb^{3+}). Hydrogen atoms are omitted for clarity.

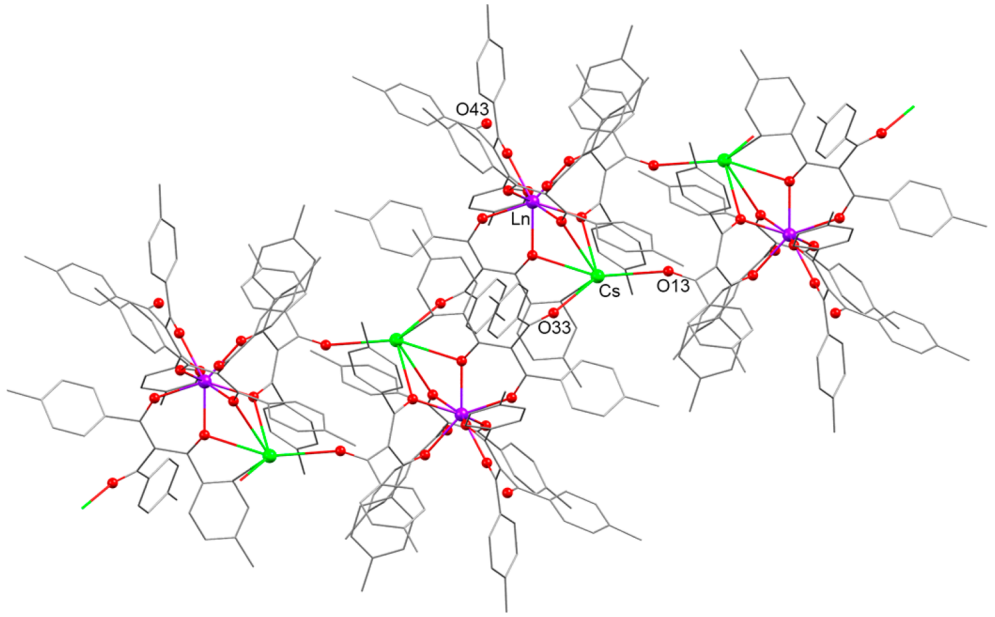

Figure 3. Representation of the X-ray crystal structure of $\{[Ln(Cs)(\mathbf{mtbm})_4]_2\}_n$ (Ln^{3+} = Eu^{3+}, Er^{3+}). Hydrogen atoms are omitted for clarity.

with 4 equiv of either **tbm**H or **mtbm**H in the presence of 4 equiv of CsOH in ethanol (Figure 1). In general, slow evaporation of the solvent over several days resulted in the deposition of crystals suitable for X-ray diffraction. The formulation of all the isolated species was further confirmed by means of elemental analysis and IR spectroscopy. In particular, the former revealed the presence of various degrees of solvation, which is typical for these bimetallic Ln^{3+}/Ae^{+} assemblies.

Structural characterization revealed the formation of unique coordination polymers with formulation $\{[Ln(Cs)(\mathbf{tbm})_4]_2\}_n$ (Ln^{3+} = Eu^{3+}, Er^{3+}, Yb^{3+}) or $\{[Ln(Cs)(\mathbf{mtbm})_4]_2\}_n$ (Ln = Eu^{3+}, Er^{3+}), upon reaction of $LnCl_3$ with CsOH and either **tbm**H or **mtbm**H (Figure 1). In each case, the repeating unit of these polymeric species was found to be a tetranuclear assembly analogous to the previously reported species obtained when the alkali metal was Na^{+}, K^{+}, or Rb^{+}.[29,31] On the other hand, reaction of $YbCl_3$ with **mtbm**H and CsOH yielded a different coordination polymer that was identified as $[Yb(Cs{\cdot}HOEt)(\mathbf{mtbm})_4]_n$ (Figure 1). In this case, the repeating unit can be more appropriately described as mononuclear Yb^{3+} complexes linearly bridged by Cs^{+} cations.

Notably, when crystals obtained from the reaction of hydrated $EuCl_3$ and **mtbm**H were analyzed, a second product was also identified by the presence of crystals having a different morphology with respect to those belonging to $\{[Eu(Cs)(\mathbf{mtbm})_4]_2\}_n$. This byproduct was identified as a linear polymer where mononuclear Eu^{3+} complexes bearing bis(4-methylbenzoyl)methanide ligands ($\mathbf{mdbm}^{-}$) were linked by Cs^{+} cations, $[Eu(Cs{\cdot}2HOEt)(\mathbf{mdbm})_4]_n$. This arrangement is analogous to a previously published structure formed by lanthanoid cations and dibenzoylmethanide.[32] The presence of this species seems to indicate possible retro-Claisen reactivity of the triketonate ligands under the alkaline reaction conditions, with formation of the analogous diketonate species. This hypothesis is supported by the fact that the ^{1}H NMR spectrum of **mtbm**H does not show the presence of **mdbm**H (see the Supporting Information).

Analogous reactions were attempted by substituting CsOH with Cs_2CO_3; however, no lanthanoid-containing species could

DOI: 10.1021/acs.inorgchem.7b00928
Inorg. Chem. 2017, 56, 8975−8985

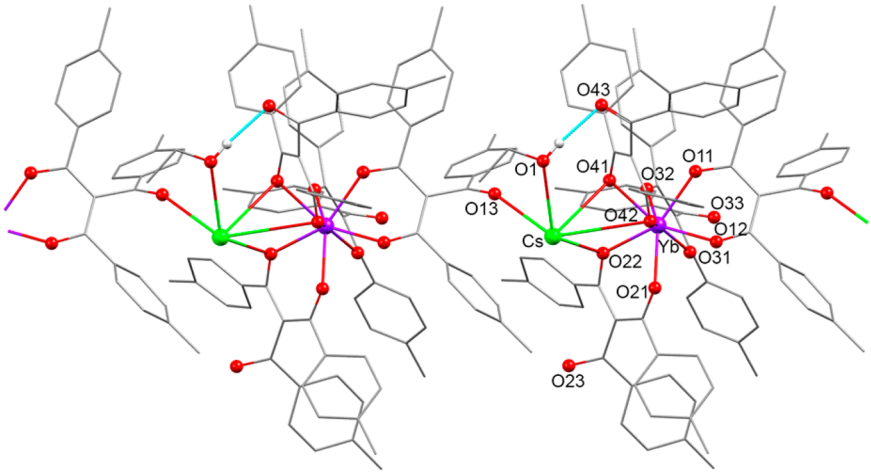

Figure 4. Representation of the X-ray crystal structure of $[Yb(Cs)(\mathbf{mtbm})_4]_n$. Hydrogen atoms are omitted for clarity. The hydrogen-bonding interaction is highlighted with a light blue line.

be identified upon deposition of the crystals. In fact, only the formation of the cesium-containing coordination polymer $[Cs(\mathbf{tbm})]_n$ was identified (see the Supporting Information for a description of this structure). The use of Cs_2CO_3 was therefore not further explored.

X-ray Diffraction Studies. The repeating units of the three $\{[Ln(Cs)(\mathbf{tbm})_4]_2\}_n$ (Ln^{3+} = Eu^{3+}, Er^{3+}, Yb^{3+}) polymers were analogous to those of previously reported Ln^{3+}/Ae^+ assemblies.[29,31] A Ln^{3+}/Cs^+ dimer is formed by two Ln^{3+} and two Cs^+ metal centers surrounded by eight anionic triketonates (Figure 2). Each Ln^{3+} ion is eight-coordinate, with the four $\mathbf{tbm}^-$ ligands binding in a bidentate mode. The third O-keto atoms of two of the ligands, O(23,43), are not involved in any contact, one O-keto atom, O(33), bridges to a Cs^+ ion to form the dimer, and the fourth, O(13), bridges to a neighboring Cs^+ to form the polymeric structure. In the previously reported dimeric structures,[29] this last position in the coordination sphere of the Ae^+ cation was occupied by the O atom of an ethanol molecule. Here, an EtOH molecule is found in the lattice, with a hydrogen bond formed with the keto O(43) atom. The remainder of the coordination sphere of the Cs^+ comprises three μ-O atoms (one each from ligands 1−3) bridging to the Ln^{3+} cation.

The structures of the two $\{[Ln(Cs)(\mathbf{mtbm})_4]_2\}_n$ (Ln^{3+} = Eu^{3+}, Er^{3+}) polymers are unsolvated and are structurally similar to the $\mathbf{tbm}^-$ coordination polymers (Figure 3). The tetranuclear Ln^{3+}/Ae^+ dimeric assembly is again observed, with the polymeric structure formed by coordination to the Cs^+ cations. The specifics of these bridging interactions between the tetranuclear assemblies do differ. On comparison of the two Eu^{3+} polymeric structures, in the $\mathbf{mtbm}^-$ system, the closest approaches between aromatic rings and the Cs^+ cations occur within the tetranuclear assembly (Cs···C(216,316), 3.324, 3.521; Cs···centroid(2,3), 3.926, 4.257 Å), consistent with an attractive interaction.[33,34] In contrast, the closest such approaches occur *between* the tetranuclear assemblies in the $\mathbf{tbm}^-$ polymers (Cs···C(115), 3.580 Å; Cs···centroid, 3.542 Å). This results in a $Cs^+\cdots Cs^+$ distance between linked tetranuclear assemblies of 7.332 Å in the $\mathbf{tbm}^-$ system, in comparison to 8.168 Å in the $\mathbf{mtbm}^-$ system.

The $[Yb(Cs)(\mathbf{mtbm})_4]_n$ polymer crystallized with a significantly different structure (Figure 4). This species is comprised of one Yb^{3+} and one Cs^+ that are counterbalanced by four anionic $\mathbf{mtbm}^-$ ligands. Each Yb^{3+} is octacoordinated and bound to four ligands in a bidentate mode. The third keto-O atoms on three of the ligands are not coordinated, while the fourth, O(13), is bridging to the Cs^+ cation. The bridging interaction also involves a close approach with the second ring of the first ligand, with a $Cs^+\cdots$centroid distance of 3.473 Å. The remainder of the coordination sphere of the Cs^+ cation includes three μ-O atoms bridging to Yb^{3+} (one from ligand 2, two from ligand 4) and a molecule of ethanol, which presents a hydrogen-bond interaction with the keto-O(43) atom (O(1)···O(43), 2.838 Å).

The $[Eu(Cs)(HOEt)_2(\mathbf{mdbm})_4]_n$ species (Figure 5), presumably formed due to a retro-Claisen reaction of $\mathbf{mtbm}^-$ in the presence of CsOH and hydrated $EuCl_3$, is a coordination polymer analogous to previous reports. Each subunit comprises one octacoordinate Eu^{3+} and one Cs^+ counterbalanced by four deprotonated ligands. The Cs^+ is coordinated to two molecules of solvent and six μ-O atoms bridging to the Eu^{3+}.

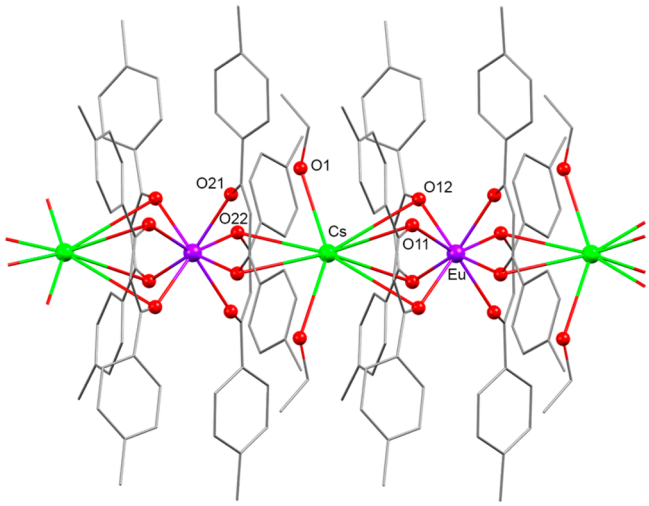

Figure 5. Representation of the X-ray crystal structure of $[Eu(Cs)(HOEt)_2(\mathbf{mdbm})_4]_n$. Hydrogen atoms are omitted for clarity.

Photophysical Properties. The photophysical data, which include excited state lifetime decay (τ_{obs}), calculated radiative decay (τ_R), intrinsic photoluminescence quantum yield (Φ_{Ln}^{Ln}),

DOI: 10.1021/acs.inorgchem.7b00928
Inorg. Chem. 2017, 56, 8975−8985

overall photoluminescence quantum yield (Φ^{L}_{Ln}), and calculated sensitization efficiency (η_{sens}), are reported in Table 1.

Table 1. Photophysical Data for the Complexes in the Solid State

complex	τ_{obs} (μs)	τ_R (ms)	Φ^{Ln}_{Ln}	Φ^{L}_{Ln} [c]	η_{sens}
$\{[Eu(Cs)(\mathbf{tbm})_4]_2\}_n$	355	0.660	0.54	0.31	0.57
$\{[Eu(Cs)(\mathbf{mtbm})_4]_2\}_n$	424	0.798	0.53	0.37	0.64
$\{[Er(Cs)(\mathbf{tbm})_4]_2\}_n$	7	0.660[a]	0.01		
$\{[Er(Cs)(\mathbf{mtbm})_4]_2\}_n$	7	0.660[a]	0.01		
$\{[Yb(Cs)(\mathbf{tbm})_4]_2\}_n$	46	1.200[b]	0.04		
$[Yb(Cs)(\mathbf{mtbm})_4]_n$	19	1.200[b]	0.01		

[a]Literature τ_R for Er^{3+}. [b]Literature τ_R for Yb^{3+}.[7] [c]Measured with the use of an integrating sphere.

The emission properties were recorded in the solid state, as we have previously demonstrated that these assemblies do not persist in polar coordinating solvents and are generally insoluble in nonpolar solvents.[29] This was also the case for species bound to the **mtbm**$^-$ ligand, as the substitution with a simple methyl group does not appear to be sufficient to impart solubility in common noncoordinating solvents. In each case, the emission of the various species originates as a consequence of the antenna effect, an argument that is supported by the broad excitation spectra that are analogous to the corresponding absorption profiles of the **tbm**$^-$ and **mtbm**$^-$ ligands (see the Supporting Information). The triplet states of **tbm**$^-$ and **mtbm**$^-$ were found to be approximately the same and in the range 21500−20500 cm^{-1} (0−phonon transition at 465−488 nm), on the basis of measurements of the phosphorescent emission at 77 K of their corresponding Gd^{3+} complexes in ethanol (see the Supporting Information).[35] The energy of the triplet state is therefore high enough to sensitize emission from the excited states of Eu^{3+}, Er^{3+}, and Yb^{3+} (the last possibly via charge transfer excited states).[16,36]

The emission spectra of $\{[Eu(Cs)(\mathbf{tbm})_4]_2\}_n$ and $\{[Eu(Cs)(\mathbf{mtbm})_4]_2\}_n$ are very similar and show the characteristic Eu^{3+}-centered linelike bands in the region 580−750 nm (Figure 6), corresponding to the $^7F_J \leftarrow {}^5D_0$ (J = 0−4) transitions. The $^7F_0 \leftarrow {}^5D_0$ peak appears narrow (full width at half-maximum smaller than ~30 cm^{-1}), albeit of very weak intensity, indicating

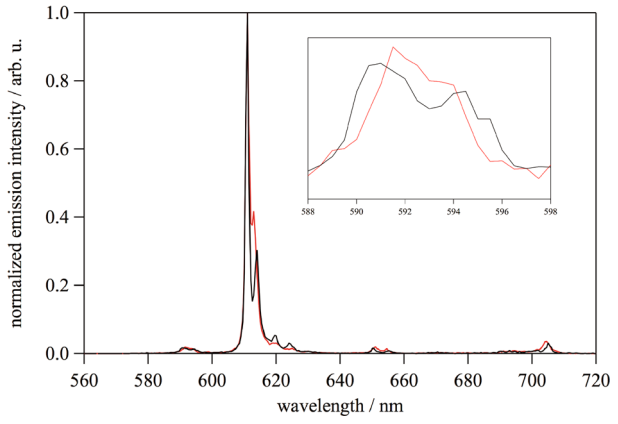

Figure 6. Normalized emission plots for $\{[Eu(Cs)(\mathbf{tbm})_4]_2\}_n$ (red trace) and $\{[Eu(Cs)(\mathbf{mtbm})_4]_2\}_n$ (black trace), with excitation wavelength at 350 nm. Inset: highlight of the peaks corresponding to the $^7F_1 \leftarrow {}^5D_0$ transition.

that the emission originates in each case from a unique Eu^{3+} and is in agreement with the fact that the two Eu^{3+} cations in each assembly unit are related by an inversion center.[7,29,37]

The magnetic dipole allowed transition, $^7F_1 \leftarrow {}^5D_0$, appears to be split into two bands in the case of $\{[Eu(Cs)(\mathbf{tbm})_4]_2\}_n$ and into three bands (with two being quasi-degenerate) for $\{[Eu(Cs)(\mathbf{mtbm})_4]_2\}_n$. This trend suggests slightly different degrees of distortion between the two coordination spheres,[37] which is supported by the results found in the shape analysis study, where $\{[Eu(Cs)(\mathbf{mtbm})_4]_2\}_n$ is more distorted than $\{[Eu(Cs)(\mathbf{tbm})_4]_2\}_n$ with respect to an ideal triangular dodecahedron (see the Supporting Information).[38] Slight differences can also be observed in the splitting of the hypersensitive $^7F_2 \leftarrow {}^5D_0$ peaks.

Excited state lifetime decay values (τ_{obs}) were measured to be 355 and 424 μs for $\{[Eu(Cs)(\mathbf{tbm})_4]_2\}_n$ and $\{[Eu(Cs)(\mathbf{mtbm})_4]_2\}_n$, respectively. In both cases, the decays were satisfactorily fitted with monoexponential functions. From the emission spectra, the values of the radiative lifetimes could be estimated at 0.660 and 0.798 ms for $\{[Eu(Cs)(\mathbf{tbm})_4]_2\}_n$ and $\{[Eu(Cs)(\mathbf{mtbm})_4]_2\}_n$, respectively. The overall quantum yields of the compounds were measured with values of 0.51 and 0.57 for $\{[Eu(Cs)(\mathbf{tbm})_4]_2\}_n$ and $\{[Eu(Cs)(\mathbf{mtbm})_4]_2\}_n$, respectively. From these data, the intrinsic quantum yields, as a ratio of τ_{obs}/τ_R, could be calculated at 0.54 and 0.53, providing information on the sensitization efficiency for the **tbm**$^-$ (0.57) and **mtbm**$^-$ ligand (0.64).

Taken together, the photophysical data for the two Eu^{3+} species indicate that in these complexes energy transfer from the **tbm**$^-$ and **mtbm**$^-$ ligands is quite efficient and is in line with the previously reported Eu^{3+} assemblies obtained with Na^+, K^+, and Rb^+.[29]

The emission spectra of both $\{[Er(Cs)(\mathbf{tbm})_4]_2\}_n$ and $\{[Er(Cs)(\mathbf{mtbm})_4]_2\}_n$ show the characteristic Er^{3+}-based NIR emission in the 1450−1650 nm spectral region. This peak is attributed to the spin-allowed $^4I_{15/2} \leftarrow {}^4I_{13/2}$ transition (Figure 7). The peak appears structured as a consequence of the crystal

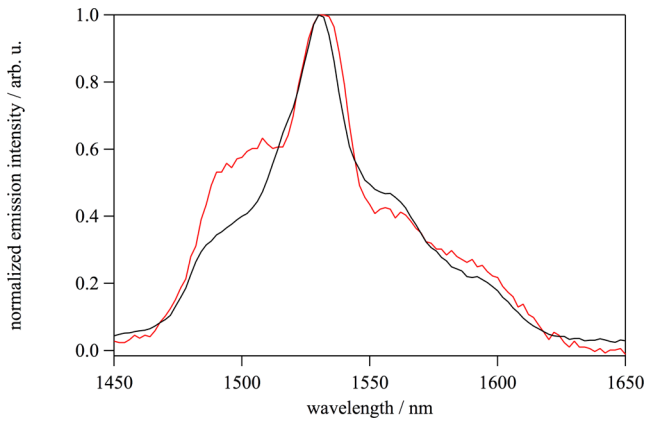

Figure 7. Normalized emission plots for $\{[Er(Cs)(\mathbf{tbm})_4]_2\}_n$ (red trace) and $\{[Er(Cs)(\mathbf{mtbm})_4]_2\}_n$ (black trace), with excitation wavelength at 350 nm.

field effect exerted by the ligands.[39] The fine structure of the splitting is slightly different, which is ascribed to a different degree of distortion in the coordination sphere around the Er^{3+} centers in the two species (see the Supporting Information).[38]

The values of τ_{obs} were measured to be 7 μs for both $\{[Er(Cs)(\mathbf{tbm})_4]_2\}_n$ and $\{[Er(Cs)(\mathbf{mtbm})_4]_2\}_n$. Both decay

DOI: 10.1021/acs.inorgchem.7b00928
Inorg. Chem. 2017, 56, 8975−8985

profiles were satisfactorily fitted by monoexponential functions (after deconvolution from instrumental response). This value provides an estimation of the intrinsic quantum yield Φ_{Ln}^{Ln} of 0.01. As in the case of the previously published assemblies bearing Er^{3+} and Na^+, K^+, or Rb^+,[29] τ_{obs} is longer than the average excited state lifetime values for Er^{3+} diketonate species (1−2 μs) and is within the range of Er^{3+} species that have complexes with perfluorinated and deuterated ligands (6−11 μs at 58−98% α-deuteration).[39,40]

Characteristic NIR emission from both $\{[Yb(Cs)(\mathbf{tbm})_4]_2\}_n$ and $[Yb(Cs{\cdot}HOEt)(\mathbf{mtbm})_4]_n$ was observed in the 900−1100 nm region, corresponding to the spin-allowed $^2F_{7/2} \leftarrow {}^2F_{5/2}$ transition (Figure 8). This transition is split into four main

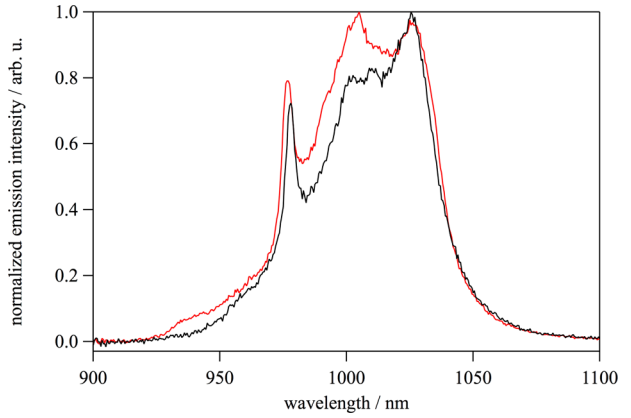

Figure 8. Normalized emission plots for $\{[Yb(Cs)(\mathbf{tbm})_4]_2\}_n$ (red trace) and $[Yb(Cs{\cdot}HOEt)(\mathbf{mtbm})_4]_n$ (black trace), with excitation wavelength at 350 nm.

bands due to crystal field effects and shows emission from hot bands as a shoulder in the 930−960 nm region.[7] As in the previous cases, slight differences in the fine splitting of the band are ascribed to a variable degree of distortion for the two Yb^{3+} centers (see the Supporting Information).[38]

The observed lifetime decays τ_{obs} were fitted to a monoexponential function and gave values of 46 and 19 μs for $\{[Yb(Cs)(\mathbf{tbm})_4]_2\}_n$ and $[Yb(Cs{\cdot}HOEt)(\mathbf{mtbm})_4]_n$, respectively. If the radiative lifetime is assumed to be 1200 μs (which is the standard assumption for Yb^{3+} diketonate complexes, but experimental data are known to range between 500 and 1200 μs),[7,41,42] the complexes would have intrinsic quantum yield values of 0.04 and 0.01, respectively. The value of τ_{obs} for $\{[Yb(Cs)(\mathbf{tbm})_4]_2\}_n$ is still relatively high in comparison to those of Yb^{3+} diketonate compounds (4−5 μs,)[43] and it is analogous to the previously reported series of Yb^{3+}/Ae^+ ($Ae^+ = Na^+$, K^+, Rb^+) assemblies.[29] This new result suggests that the presence of the molecule of ethanol coordinated to Ae^+ in the tetranuclar assemblies is not a dominant factor for nonradiative deactivation of the $^2F_{5/2}$ excited state of Yb^{3+}. Interestingly, the $[Yb(Cs{\cdot}HOEt)(\mathbf{mtbm})_4]_n$ species has a composition similar to that of the tetranuclear assemblies, but its excited state lifetime is halved. On the basis of the previous consideration, it might be excluded that the shorter value of τ_{obs} for $[Yb(Cs{\cdot}HOEt)(\mathbf{mtbm})_4]_n$ will be due to multiphonon relaxation caused by the molecule of ethanol coordinated to the Cs^+ cation. Given that energy migration is unlikely due to the distance between Yb^{3+} centers,[41] the difference in excited state lifetime decays could be caused by a shorter value of τ_R for $[Yb(Cs{\cdot}HOEt)(\mathbf{mtbm})_4]_n$, and this aspect is currently under investigation.

To gain a more detailed insight into the kinetics involved in the sensitization process for the triketonate ligands, we have also performed transient absorption (TA) measurements on the femtosecond time scale, which have proven useful in understanding the excited state properties for diketonate species.[44−47] However, as noted earlier, we have shown that the tetranuclear assemblies do not persist in polar coordinating solvents,[29] which necessitated these measurements to be

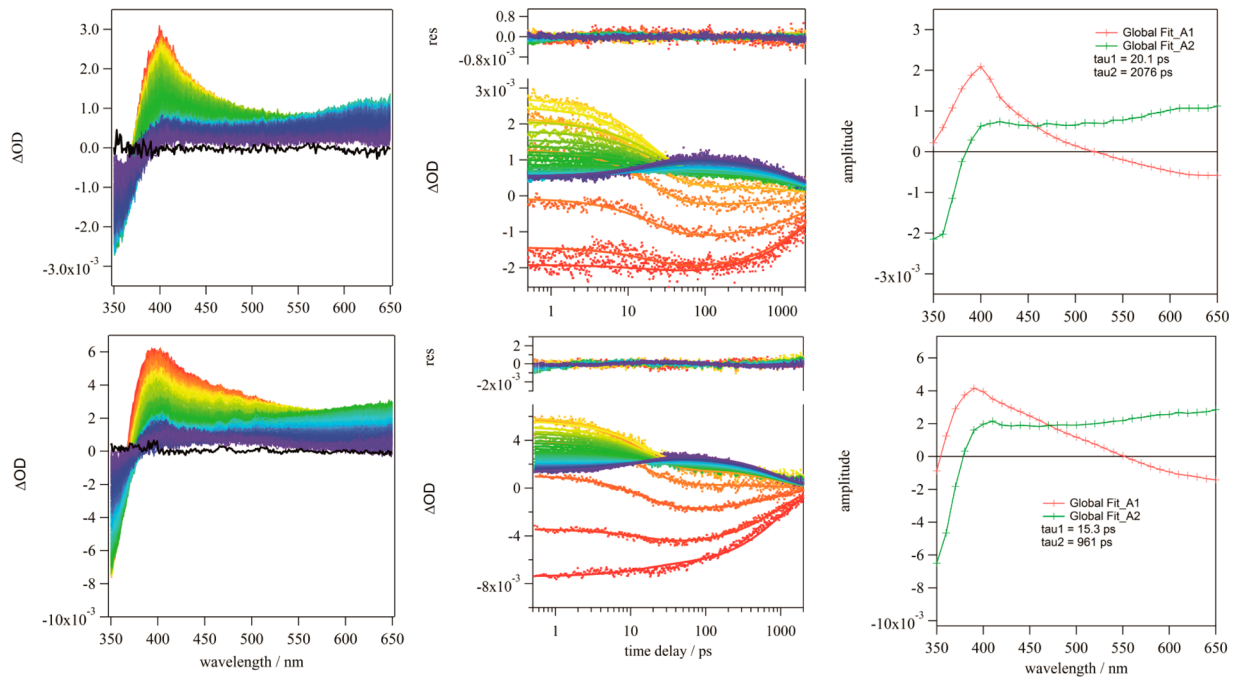

Figure 9. TA spectra (left) of Gd^{3+} complexes of $\mathbf{mtbm}^-$ (top) and $\mathbf{tbm}^-$ (bottom), along with corresponding decay kinetic plots (middle) and decay associated difference spectra (right).

DOI: 10.1021/acs.inorgchem.7b00928
Inorg. Chem. 2017, 56, 8975−8985

Table 2. Summary of Excited State Properties Determined by fs-TA Spectroscopy

complex	$\tau_1(S_1 \rightarrow S_n)$ (ps)	$k_{obs\text{-}S1}$ (s^{-1})	$\tau_2(T_1 \rightarrow T_n)$ (ps)	$k_{obs\text{-}T1}$ (s^{-1})	$k_{EET\text{-}T1}$ (s^{-1})	$\Phi_{EET\text{-}T1}$ (%)
$[Gd(\mathbf{tbm})]^{2+}$	15.3	6.54×10^{10}	961	1.04×10^{9}		
$[Gd(\mathbf{mtbm})]^{2+}$	20.1	4.98×10^{10}	2076	4.82×10^{8}		
$[Yb(\mathbf{tbm})]^{2+}$	2.4	4.17×10^{11}	28.4	3.52×10^{10}	3.42×10^{10}	97.0
$[Yb(\mathbf{mtbm})]^{2+}$	4.4	2.27×10^{11}	72.0	1.39×10^{10}	1.34×10^{10}	96.5
$[Er(\mathbf{tbm})]^{2+}$	7.2	1.39×10^{11}	37.4	2.67×10^{10}	2.57×10^{10}	96.1
$[Er(\mathbf{mtbm})]^{2+}$	5.4	1.85×10^{11}	36.5	2.74×10^{10}	2.69×10^{10}	98.2
$[Eu(\mathbf{tbm})]^{2+}$	5.1	1.96×10^{11}				
$[Eu(\mathbf{mtbm})]^{2+}$	4.3	2.33×10^{11}				

performed using simpler model complexes. To that end, solutions of the **tbm**$^-$ and **mtbm**$^-$ ligands were prepared using a K_2CO_3-saturated EtOH solution as the solvent, in order to ensure deprotonation of the ligand in solution. To these solutions was added a large molar excess (>10 equiv) of the Ln^{3+} = Gd^{3+}, Eu^{3+}, Yb^{3+}, Er^{3+} cation as their trifluoromethanesulfonate salts. Formation of 1:1 $[Ln(\mathbf{tbm})(H_2O)_x]^{2+}$ and $[Ln(\mathbf{mtbm})(H_2O)_x]^{2+}$ complexes was confirmed using UV−vis spectroscopy, which showed a shift in the absorption peak maxima to ca. 340 nm upon metal ion complexation.

The resulting TA spectra for the Gd^{3+} complexes of **tbm**$^-$ and **mtbm**$^-$ are shown in Figure 9. The excited state difference spectra (ΔOD) at early time delays reveal a negative ground state bleach (GSB) signal at wavelengths less than 380 nm and a positive excited state absorption (ESA) peak centered at ca. 400 nm, with the latter decaying rapidly to form a more broad feature centered at ca. 650 nm, which subsequently decays. The corresponding kinetic plots for the observed ΔOD dynamics integrated over 10 nm data intervals from 350 to 650 nm are shown in Figure 9, and these data were globally fit to a biexponential decay function of the form

$$I_t = A_1 \exp^{-1/\tau_1 t} + A_2 \exp^{-1/\tau_2 t}$$

where I_t is the intensity of the transient absorption data at time t, τ_1 and τ_2 are the observed lifetimes, and A_1 and A_2 are pre-exponential scaling factors. The best fit to the experimental data are shown in Figure 9, and resulting lifetimes are summarized in Table 2, together with the decay associated difference spectra (DADS) shown in Figure 9.

Notably, the data for the Gd^{3+} complexes of **tbm**$^-$ and **mtbm**$^-$ are very similar, which is not surprising given their chemical structures. For both complexes, a fast decay component (τ_1 = 15−20 ps) at *ca* 400 nm (positive DADS signal) is matched by a fast rise at *ca* 650 nm (negative DADS signal). Hence, these spectral features may be assigned to decay of the initially populated S_1 excited state to form the T_1 excited state via ISC, with subsequent decay of the T_1 state on the nanosecond time scale leading to ground state recovery.

Corresponding data for the remaining Ln^{3+} = Eu^{3+}, Er^{3+}, and Yb^{3+} complexes of the **tbm**$^-$ and **mtbm**$^-$ ligands were also collected and are shown in the Supporting Information. For the Yb^{3+} and Er^{3+} complexes, the spectra obtained are again very similar and yielded excellent fits to a biexponential decay model. As summarized in Table 2, the evaluated decay lifetimes for both the S_1 and T_1 excited states of these complexes are shorter than those for the corresponding Gd^{3+} complexes, indicating efficient ISC and energy transfer to the corresponding 4f* accepting states.

Using the Gd^{3+} complexes as model compounds, and assuming the other radiative and nonradiative decay pathways will be equivalent for the Ln^{3+} complexes, we are able to calculate the rate of electronic energy transfer from the excited T_1 state ($k_{EET\text{-}T1}$) and hence the efficiencies for this triplet-mediated sensitization pathway ($\Phi_{EET\text{-}T1}$), which are summarized in Table 2. The calculated rate constants are on the order of ∼10^{10} s^{-1} and reveal that both the **tbm**$^-$ and **mtbm**$^-$ ligands are efficient sensitizers, with $\Phi_{EET\text{-}T1}$ values of ≥96%.

For the corresponding Eu^{3+} complexes, a close analysis of the TA spectra revealed a very interesting result. For both the **tbm**$^-$ and **mtbm**$^-$ ligands, while the initial ΔOD spectra obtained at early time delays were similar to those for the other complexes, the broader spectral feature appearing at ca. 650 nm due to $T_1 \rightarrow T_n$ excited state absorption was clearly absent, and in both cases the observed TA kinetics were more accurately represented by a monoexponential decay function of the form

$$I_t = A_1 \exp^{-1/\tau_1 t}$$

The lack of an observed $T_1 \rightarrow T_n$ signal suggests that ISC to form the excited T_1 state may be less efficient for these complexes and furthermore that either a singlet mediated energy transfer pathway and/or a competing ligand to metal charge transfer (LMCT) pathway, involving the formation of reduced Eu^{2+}, may play an important role in the sensitization of Eu^{3+} observed using these ligands. This result is in line with recent reports that have highlighted the importance of the LMCT state in sensitized Eu^{3+} luminescence.[7,14,37] However, it should also be recognized that the situation may differ in the isolated solid $\{[Ln(Cs)(\mathbf{tbm})_4]_2\}_n$ and $\{[Ln(Cs)(\mathbf{mtbm})_4]_2\}_n$ coordination polymers, since differences in the redox potential (and hence LMCT excited state energies) would be expected when comparing the tetranuclear assemblies in the solid state and the analogous simple model complexes in solution.

CONCLUSION

This work has focused on synthesizing bimetallic assemblies composed of Ln^{3+} cations (Eu^{3+}, Er^{3+}, and Yb^{3+}), Cs^+ cations, and triarylmethanide ligands. The ligands of choice were tribenzoylmethanide and tris(4-methylbenzoyl)methanide. In the case of Eu^{3+} and Er^{3+}, structural assemblies were obtained that are analogous to those in the previously reported study when Na^+, K^+, and Rb^+ were used as alkali-element cations. However, in the present work these assemblies are the repeating units of one-dimensional polymers. These units are linked through the Cs^+ cations binding to the O atoms of the triketonate ligands. The only exception to this series was the structure obtained by combining Yb^{3+}, Cs^+, and tris(4-methylbenzoyl)methanide. In this case, the repeating unit of the linear polymer was represented by mononuclear Yb^{3+} complexes bridged together via coordination of Cs^+ cations. The photophysical properties were investigated by means of absorption, emission, and transient absorption spectroscopy. In particular for Er^{3+} and Yb^{3+}, the transient absorption data reveal

DOI: 10.1021/acs.inorgchem.7b00928
Inorg. Chem. 2017, 56, 8975−8985

efficient and fast energy transfer from the triplet excited state of the ligand after ISC. On the other hand, the transient absorption data for Eu^{3+} seems to suggest an alternative energy transfer pathway, occurring either directly via the ligand singlet state or through the population of an intermediate LMCT state. The emission profiles, excited state lifetimes, and quantum yield data for the Eu^{3+} species confirm efficient sensitization and relatively high quantum yields, with values in line those for previously reported Eu^{3+} diketonate complexes. On the other hand, the NIR emission of Er^{3+} and Yb^{3+} highlights rather elongated excited state lifetimes with respect to analogous diketonate species, similar to those previously observed for assemblies of these elements, tribenzoylmethanide, and Na^+, K^+, or Rb^+. This work concludes the series of Ln^{3+}/Ae^+ assemblies and reinforces our previous results confirming that these species constitute viable building blocks for the preparation of efficient NIR emitters.

EXPERIMENTAL SECTION

General Procedures. All reagents and solvents were purchased from chemical suppliers and used as received without further purification. The ligand tribenzoylmethane (**tbm**H) was prepared as previously reported.[31] Hydrated $LnCl_3$ (Ln = Eu^{3+}, Er^{3+}, Yb^{3+}) was prepared by the reaction of Ln_2O_3 with hydrochloric acid (5 M), followed by evaporation of the solvent under reduced pressure. Infrared spectra (IR) were recorded on solid-state samples using an attenuated total reflectance PerkinElmer Spectrum 100 FT-IR instrument. IR spectra were recorded from 4000 to 650 cm^{-1}; the intensities of the IR bands are reported as strong (s), medium (m), or weak (w), with broad (br) bands also specified. Melting points were determined using a BI Barnsted Electrothermal 9100 apparatus. Elemental analyses were obtained at Curtin University, Bentley, Australia. Nuclear magnetic resonance (NMR) spectra were recorded using a Bruker Avance 400 spectrometer (400.1 MHz for ^1H; 100 MHz for ^{13}C) at 300 K. The data were acquired and processed by the Bruker TopSpin 3.1 software. All of the NMR spectra were calibrated to residual solvent signals.

Selected Equations. The values of the radiative lifetime (τ_R) and intrinsic quantum yield (Φ^{Ln}_{Ln}), can be calculated with the equations[37]

$$\frac{1}{\tau_R} = 14.65\ s^{-1} \times n^3 \times \frac{I_{tot}}{I_{MD}} \quad (1)$$

$$\Phi^{Ln}_{Ln} = \frac{\tau_{obs}}{\tau_R} \quad (2)$$

In eq 1, the refractive index (n) of the solvent is used (assumed value of 1.5 in the solid state), The value 14.65 s^{-1} is the spontaneous emission probability of the $^7F_1 \leftarrow {}^5D_0$ transition reported previously. I_{tot} is the total integration of the Eu^{3+} emission spectrum, and I_{MD} is the integration of the $^7F_1 \leftarrow {}^5D_0$ transition. The sensitization efficiency (η_{sens}) can be determined using eq 3:

$$\eta_{sens} = \frac{\Phi^{L}_{Ln}}{\Phi^{Ln}_{Ln}} \quad (3)$$

Photophysical Measurements. Absorption spectra were recorded at room temperature using a PerkinElmer Lambda 35 UV/vis spectrometer. Uncorrected steady-state emission and excitation spectra were recorded using an Edinburgh FLSP980-stm spectrometer equipped with a 450 W xenon arc lamp, double excitation and emission monochromators, a Peltier cooled Hamamatsu R928P photomultiplier (185−850 nm), and a Hamamatsu R5509-42 photomultiplier for detection of NIR radiation (800−1400 nm). Emission and excitation spectra were corrected for source intensity (lamp and grating) and emission spectral response (detector and grating) by a calibration curve supplied with the instrument. Quantum yields were measured with the use of an integrating sphere coated with BenFlect.[48] Experimental uncertainties are estimated to be ±15% for quantum yields.

Excited-state decays (τ) were recorded on the same Edinburgh FLSP980-stm spectrometer using a microsecond flashlamp. The goodness of fit was assessed by minimizing the reduced χ^2 function and by visual inspection of the weighted residuals. Experimental uncertainties are estimated to be ±8% for lifetime determinations.

To record the luminescence spectra at 77 K, the samples were placed in quartz tubes (2 mm diameter) and inserted in a special quartz Dewar filled with liquid nitrogen. All of the solvents used in the preparation of the solutions for the photophysical investigations were of spectrometric grade.

Transient Absorption Measurements. The excitation source utilized for femtosecond transient absorption measurements was an amplified laser system (Spitfire ACE, Spectra Physics) delivering 800 nm laser pulses of 110 fs duration and a 1 kHz repetition rate. Approximately 0.1 mJ of this output was attenuated and focused onto a 15 mm CaF_2 window mounted on an automated z-stage translation mount to generate a white light continuum probe pulse from 350 to 650 nm. The remainder of the laser fundamental was coupled to an OPA system (Topas Prime, Light Conversion) which was tuned to deliver excitation pulses at 340 nm. The pump pulse polarization was set to magic angle with respect to the probe, and ground and excited state difference spectra (ΔOD) at various delay times were measured using a femtosecond TA spectrometer (Helios, Ultrafast Systems) incorporating two 512 pixel CCD sensors as the sample and reference channel. Sample absorbances were ca. 0.4 over the 2 mm path length cell used, and these were continuously stirred mechanically. No detectable changes were observed in the UV−vis absorption spectrum of the complex at the completion of transient absorption studies, indicating no decomposition. The instrument response function (IRF) had a full width at half-maximum (fwhm) of ca. 200 fs, measured experimentally by a Gaussian fit to the scattered laser excitation profile, and spectra were corrected for the chirp of the probe pulses. The resulting time traces were analyzed globally using commercially available software (Igor, Version 6.1.2.1, Wavemetrics). Experimental uncertainties are estimated to be ±10% for lifetime determinations.

Synthesis of Bis(4-methylbenzoyl)methane (mdbmH). The **mdbm**H precursor was synthesized following a slightly modified procedure.[49] Ethyl 4-methylbenzoate (500 mg, 3 mmol) and 4-acetyltoluene (400 mg, 3 mmol) were combined in 40 mL of THF. To this solution, a suspension of NaH (60% in mineral oil, 360 mg, 9.0 mmol) in 40 mL THF was added dropwise at 0 °C. After 1 h, the combined mixture was heated to 40 °C for 16 h under a nitrogen atmosphere. The solvent was then removed under reduced pressure, and water (20 mL) was added to the residual solid paste. The pH was adjusted approximately to neutral by addition of HCl solution (1 M). The aqueous phase was then extracted with ethyl acetate (3 × 15 mL), and the combined organic phase was dried over $MgSO_4$. After filtration, the crude product was obtained by removal of the solvent under reduced pressure and the target compound was isolated following purification via recrystallization in ethanol as a yellow solid. Yield: 80%. The spectroscopic data match those previously reported.[49]

Synthesis of Tris(4-methylbenzoyl)methane (mtbmH). 4-Methylbenzoic acid (625 mg, 4.8 mmol) was added to thionyl chloride (5 mL) and heated at reflux for 2 h. After this time, the solvent was removed under reduced pressure and the remaining solid 4-methylbenzoyl chloride was immediately added to diethyl ether (20 mL). NaH (60% in mineral oil, 144 mg, 3.6 mmol) and **mdbm**H (300 mg, 1.2 mmol) were combined in 20 mL of diethyl ether, and the suspension was maintained at 0 °C. To this suspension was added a solution of 4-methylbenzoyl chloride in diethyl ether dropwise. After the addition, the mixture was stirred under a nitrogen atmosphere at 40 °C for 16 h. The formed precipitate was filtered and washed with a HCl solution (1 M). The solid was then dried under reduced pressure for several hours and afforded the target compound as a white solid. Yield: 60%. Mp: 233−234 °C. Anal. Calcd for $C_{25}H_{22}O_3$: C, 80.67; H, 6.01. Found: C, 80.61; H, 5.93. IR (ATR): ν 2920 w, 1685 s, 1669 s, 1605 s, 1574 w, 1509 w, 1446 w, 1406 w, 1376 w, 1316 m, 1284 s, 1260 m, 1218 m, 1192 m, 1181 s, 1123 w, 1020 m, 1011 m, 957 w, 906

DOI: 10.1021/acs.inorgchem.7b00928
Inorg. Chem. 2017, 56, 8975−8985

w, 859 s, 841 w, 815 s, 783 w, 711 m cm^{-1}. ^1H NMR (400 MHz, DMSO-d_6): δ 7.95 (s, 1H, αCH), 7.89 (d, J = 8.0 Hz, 6H, H_{ortho}), 7.35 (d, J = 8.0 Hz, 6H, H_{meta}), 2.38 (s, 9H, CH_3) ppm. ^{13}C NMR(101 MHz, DMSO-d_6) δ 193.3 (CO), 144.9 (αCH), 133.3 (C1), 129.7 (C_{ortho}), 128.9 (C_{meta}), 65.1 (C_{para}), 21.4 (CH_3) ppm.

General Procedure for the Synthesis of Lanthanoid Assemblies. CsOH (4 equiv) was added to a mixture containing **mtbm**H or **tbm**H (4 equiv) and hydrated $LnCl_3$ (ca. 20 mg) in ethanol (10 mL). The mixture was heated at reflux for 30 min and filtrered over a glass frit while still hot. The filtered solution was then left undisturbed at ambient temperature, and slow evaporation of the solvent over several days afforded crystals suitable for X-ray diffraction.

*{[Eu(Cs)(**tbm**)$_4$]$_2$}$_n$*. Mp 271−272 °C. Anal. Calcd for $C_{88}H_{60}CsO_{12}Eu$: C, 66.30; H, 3.79. Found: C, 65.93; H, 3.31. IR (ATR): ν 3057 w, 1646 w, 1584 m, 1545 s, 1446 m, 1368 s, 1273 m, 1153 m, 1073 w, 1027 w, 1013 w, 924 w, 896 s, 823 m, 780 m, 744 m, 693 s, 666 m cm^{-1}.

*{[Er(Cs)(**tbm**)$_4$]$_2$}$_n$*. Mp 260−261 °C. Anal. Calcd for $C_{88}H_{60}CsO_{12}Er{\cdot}1.6H_2O$: C, 64.51; H, 3.89. Found: C, 64.00; H, 3.31. IR (ATR): ν 3056 w, 1646 w, 1585 m, 1548 s, 1446 m, 1371 s, 1275 m, 1153 m, 1073 w, 1027 w, 1013 w, 924 w, 896 s, 823 m, 780 m, 743 m, 693 s, 667 m cm^{-1}.

*{[Yb(Cs)(**tbm**)$_4$]$_2$}$_n$*. Mp 252−253 °C. Anal. Calcd for $C_{88}H_{60}CsO_{12}Er{\cdot}0.3H_2O$: C, 65.18; H, 3.37. Found: C, 64.70; H, 3.36. IR (ATR): ν 3056 w, 3026 w, 1646 w, 1585 m, 1550 s, 1446 m, 1372 s, 1313 m, 1274 m, 1177 w, 1154 m, 1103 w, 1073 w, 1027 w, 1013 w, 1000 w, 973 w, 924 w, 896 s, 823 m, 811 w, 780 m, 743 m, 693 s, 667 m cm^{-1}.

*{[Eu(Cs)(**mtbm**)$_4$]$_2$}$_n$*. Mp 291−290 °C. Anal. Calcd for $C_{100}H_{84}O_{12}EuCs{\cdot}2H_2O$: C, 66.78; H, 4.93. Found: C, 66.36; H, 4.49. IR (ATR): ν 3058 w, 3024 w, 1642 m, 1583 s, 1537 s, 1448 m, 1428 m, 1366 s, 1310 m, 1292 m, 1275 m, 1176 w, 1154 m, 1101 w, 1072 w, 1027 w, 1013 w, 1000 w, 968 w, 920 w, 895 m, 863 w, 844 w, 823 w, 810 w, 780 w, 743 m, 729 w, 721 w, 692 m, 667 w cm^{-1}.

*{[Er(Cs)(**mtbm**)$_4$]$_2$}$_n$*. Mp 298−299 °C. Anal. Calcd for $C_{100}H_{84}CsO_{12}Er$: C, 66.54; H, 4.86. Found: C, 66.43; H, 4.46. IR (ATR): ν 3057 w, 3027 w, 1646 w,1595 m, 1585 m, 1549 s, 1447 m, 1373 s, 1312 m, 1276 m, 1219 w, 1178 w, 1154 m, 1073 w, 1000 w, 972 w, 924 w, 896 m, 847 w, 823 w, 781 w, 743 m, 692 s, 668 m cm^{-1}.

*[Yb(Cs)(**mtbm**)$_4$]$_n$*. Mp 278−279 °C. Anal. Calcd for $C_{100}H_{84}O_{12}Yb{\cdot}4.5H_2O$: C, 64.41; H, 5.03. Found: C, 64.09; H, 4.53. IR (ATR): ν 3023 w, 2920 w, 1635 m, 1603 m, 1577 m, 1538 s, 1452 w, 1407 m, 1360 s, 1316 m, 1308 m, 1281 m, 1183 m, 1154 m, 1113 w, 1033 w, 1013 w, 961 w, 900 s, 850 m, 824 m, 781 s, 762 m, 734 w, 723 m, 690 w cm^{-1}.

X-ray Crystallography. Crystallographic data for the structures were collected at 100(2) K on an Oxford Diffraction Gemini or Xcalibur diffractometer fitted with Mo Kα or Cu Kα radiation. Following absorption corrections and solution by direct methods, the structures were refined against F^2 with full-matrix least squares using the program SHELX-2014.[50]

Unless stated below, anisotropic displacement parameters were employed for the non-hydrogen atoms. All hydrogen atoms were added at calculated positions and refined by use of a riding model with isotropic displacement parameters based on those of the parent atom. CCDC-1539972 ([Eu(Cs)(**tbm**)$_4$]$_n$), CCDC-1539973 ([Er(Cs)(**tbm**)$_4$]$_n$). CCDC-1539974 ([Yb(Cs)(**tbm**)$_4$]$_n$), CCDC-1539975 ([Eu(Cs)(**mtbm**)$_4$]$_n$), CCDC-1539976 ([Er(Cs)(**mtbm**)$_4$]$_n$), CCDC-1539977 ([Yb(Cs)(**mtbm**)$_4$]$_n$), CCDC-1539978 ([Eu(Cs)(EtOH)$_2$(**mdbm**)$_4$]$_n$), and CCDC-1539979 ([Cs(**tbm**)]$_n$) contain supplementary crystallographic data.

X-ray Data Refinement. *{[Eu(Cs)(**tbm**)$_4$]$_2$}$_n$*: empirical formula $C_{88}H_{60}CsEuO_{12}$, C_2H_6O; MW = 1640.29, colorless plate, 0.32 × 0.28 × 0.02 mm^3, triclinic, space group $P\bar{1}$, a = 14.6063(4) Å, b = 16.8300(4) Å, c = 17.6843(4) Å, α = 74.721(2)°, β = 77.698(2)°, γ = 83.202(2)°, V = 4088.34(17) $Å^3$, Z = 2, D_c = 1.332 g/cm^3, μ = 1.266 mm^{-1}, F_{000} = 1656, Mo Kα radiation, λ = 0.71073 Å, T = 100(2) K, $2\theta_{max}$ = 64.5°, 90077 reflections collected, 26973 unique reflections (R_{int} = 0.0599), final GOF = 1.005, R1 = 0.0485, wR2 = 0.1002, R indices based on 20172 reflections with $I > 2\sigma(I)$ (refinement on F^2), $|\Delta\rho|_{max}$ = 1.3(1) e $Å^{-3}$, 944 parameters, 6 restraints.

*{[Er(Cs)(**tbm**)$_4$]$_2$}$_n$*: empirical formula $C_{88}H_{60}O_{12}CsEr$, C_2H_6O; MW = 1655.59, colorless plate, 0.30 × 0.26 × 0.10 mm^3, triclinic, space group $P\bar{1}$, a = 14.6999(2) Å, b = 16.6792(3) Å, c = 17.5946(3) Å, α = 75.643(2)°, β = 76.758(2)°, γ = 83.394(1)°, V = 4060.28(11) $Å^3$, Z = 2, D_c = 1.354 g/cm^3, μ = 1.536 mm^{-1}, F_{000} = 1666, Mo Kα radiation, λ = 0.71073 Å, T = 100(2) K, $2\theta_{max}$ = 69.2°, 108898 reflections collected, 32735 unique reflections (R_{int} = 0.0359), final GOF = 1.004, R1 = 0.0415, wR2 = 0.1026, R indices based on 26538 reflections with $I > 2\sigma(I)$ (refinement on F^2), $|\Delta\rho|_{max}$ = 1.9(1) e $Å^{-3}$, 946 parameters, 24 restraints.

*{[Yb(Cs)(**tbm**)$_4$]$_2$}$_n$*: empirical formula $C_{88}H_{60}CsO_{12}Yb$, C_2H_6O; MW = 1661.37, colorless plate, 0.29 × 0.17 × 0.06 mm^3, triclinic, space group $P\bar{1}$, a = 14.7042(3) Å, b = 16.6321(3) Å, c = 17.6009(4) Å, α = 75.677(2)°, β = 76.631(2)°, γ = 83.400(2)°, V = 4050.07(14) $Å^3$, Z = 2, D_c = 1.362 g/cm^3, μ = 1.658 mm^{-1}, F_{000} = 1670, Mo Kα radiation, λ = 0.71073 Å, T = 100(2) K, $2\theta_{max}$ = 64.6°, 84523 reflections collected, 26691 unique reflections (R_{int} = 0.0437), final GOF = 1.010, R1 = 0.0426, wR2 = 0.1041, R indices based on 21048 reflections with $I > 2\sigma(I)$ (refinement on F^2), $|\Delta\rho|_{max}$ = 1.8(1) e $Å^{-3}$, 948 parameters, 12 restraints.

*{[Eu(Cs)(**mtbm**)$_4$]$_2$}$_n$*: empirical formula $C_{100}H_{84}CsEuO_{12}$; MW = 1762.54, colorless needle, 0.13 × 0.05 × 0.03 mm^3, triclinic, space group $P\bar{1}$, a = 14.8674(5) Å, b = 16.1731(5) Å, c = 18.0171(6) Å, α = 84.406(2)°, β = 74.987(3)°, γ = 87.816(2)°, V = 4164.1(2) $Å^3$, Z = 2, D_c = 1.406 g/cm^3, μ = 9.255 mm^{-1}. F_{000} = 1796, Cu Kα radiation, λ = 1.54178 Å, T = 100(2)K, $2\theta_{max}$ = 134.9°, 40590 reflections collected, 14792 unique reflections (R_{int} = 0.0490), final GOF = 1.001, R1 = 0.0370, wR2 = 0.0833, R indices based on 12187 reflections with $I > 2\sigma(I)$ (refinement on F^2), $|\Delta\rho|_{max}$ = 1.05(9) e $Å^{-3}$, 1027 parameters, 0 restraints.

*{[Er(Cs)(**mtbm**)$_4$]$_2$}$_n$*: empirical formula $C_{100}H_{84}CsErO_{12}$; MW = 1777.84, colorless needle, 0.28 × 0.12 × 0.05 mm^3, triclinic, space group $P\bar{1}$, a = 14.8243(3) Å, b = 16.1860(4) Å, c = 17.9760(4) Å, α = 83.768(2)°, β = 75.176(2)°, γ = 87.485(2)°, V = 4144.49(17) $Å^3$, Z = 2, D_c = 1.425 g/cm^3, μ = 1.509 mm^{-1}, F_{000} = 1806, Mo Kα radiation, λ = 0.71073 Å, T = 100(2) K, $2\theta_{max}$ = 64.4°, 92120 reflections collected, 27193 unique reflections (R_{int} = 0.0591), final GOF = 1.003, R1 = 0.0455, wR2 = 0.0998, R indices based on 20682 reflections with $I > 2\sigma(I)$ (refinement on F^2), $|\Delta\rho|_{max}$ = 2.6(1) e $Å^{-3}$, 1027 parameters, 6 restraints.

*[Yb(Cs)(**mtbm**)$_4$]$_n$*: empirical formula $C_{102}H_{90}CsO_{13}Yb$; MW = 1829.68, colorless prism, 0.23 × 0.15 × 0.13 mm^3, triclinic, space group $P\bar{1}$, a = 11.5606(2) Å, b = 16.2195(3) Å, c = 26.5428(5) Å, α = 81.060(2)°, β = 83.329(2)°, γ = 81.209(2)°, V = 4836.93(15) $Å^3$, Z = 2, D_c = 1.256 g/cm^3, μ = 1.395 mm^{-1}, F_{000} = 1862, Mo Kα radiation, λ = 0.71073 Å, T = 100(2) K, $2\theta_{max}$ = 52.7°, 81814 reflections collected, 19778 unique reflections (R_{int} = 0.0415), final GOF = 1.005, R1 = 0.0336, wR2 = 0.0810, R indices based on 17759 reflections with $I > 2\sigma(I)$ (refinement on F^2), $|\Delta\rho|_{max}$ = 1.26(8) e $Å^{-3}$, 1066 parameters, 6 restraints.

*[Eu(Cs)(EtOH)$_2$(**mdbm**)$_4$]$_n$*: empirical formula $C_{72}H_{72}CsEuO_{10}$; MW = 1382.16, colorless plate, 0.18 × 0.15 × 0.06 mm^3, monoclinic, space group $C2/c$, a = 29.9314(14) Å, b = 8.4707(3) Å, c = 26.1484(11) Å, β = 105.325(5)°, V = 6393.9(5) $Å^3$, Z = 4, D_c = 1.436 g/cm^3, μ = 11.859 mm^{-1}, F_{000} = 2808, Cu Kα radiation, λ = 1.54178 Å, T = 100(2) K, $2\theta_{max}$ = 134.3°, 15957 reflections collected, 5670 unique reflections (R_{int} = 0.0398), final GOF = 1.022, R1 = 0.0650, wR2 = 0.1834, R indices based on 4887 reflections with $I > 2\sigma(I)$ (refinement on F^2), $|\Delta\rho|_{max}$ = 2.8(2) e $Å^{-3}$, 397 parameters, 4 restraints.

*[Cs(**tbm**)]$_n$*: Empirical formula $C_{22}H_{15}CsO_3$; MW = 460.25, colorless prism, 0.63 × 0.48 × 0.20 mm^3, monoclinic, space group $P2_1/n$, a = 7.0968(1) Å, b = 15.2205(1) Å, c = 16.7822(1) Å, β = 99.828(1)°, V = 1786.16(3) $Å^3$, Z = 4, D_c = 1.712 g/cm^3, μ = 2.092 mm^{-1}, F_{000} = 904, Mo Kα radiation, λ = 0.71073 Å, T = 100(2) K, $2\theta_{max}$ = 77.9°, 68792 reflections collected, 10066 unique reflections (R_{int} = 0.0234), final GOF = 1.103, R1 = 0.0180, wR2 = 0.0449, R indices based on 9419 reflections with $I > 2\sigma(I)$ (refinement on F^2), $|\Delta\rho|_{max}$ = 0.84(8) e $Å^{-3}$, 235 parameters, 0 restraints.

DOI: 10.1021/acs.inorgchem.7b00928
Inorg. Chem. 2017, 56, 8975−8985

■ ASSOCIATED CONTENT

Supporting Information

The Supporting Information is available free of charge on the ACS Publications website at DOI: 10.1021/acs.inorgchem.7b00928.

Details of ^{1}H and ^{13}C spectra for **mtbm**H, absorption profiles for **mtbm**H and **mtbm**$^{-}$ in ethanol, emission profiles for **mtbm**H and the Gd^{3+} complex of **mtbm**H^{-} from a frozen ethanol solution at 77 K, transient absorption spectra of Ln^{3+} (Ln^{3+} = Eu^{3+}, Er^{3+}, Yb^{3+}) complexes of **tbm**$^{-}$ and **mtbm**$^{-}$, along with corresponding decay kinetic plots and decay associated difference spectra, geometrical parameters for the complexes using shape analysis, and normalized excitation and emission plots for the assemblies in the solid state (PDF)

Accession Codes

CCDC 1539972−1539979 contain the supplementary crystallographic data for this paper. These data can be obtained free of charge via www.ccdc.cam.ac.uk/data_request/cif, or by emailing data_request@ccdc.cam.ac.uk, or by contacting The Cambridge Crystallographic Data Centre, 12 Union Road, Cambridge CB2 1EZ, UK; fax: +44 1223 336033.

■ AUTHOR INFORMATION

Corresponding Authors

*E-mail for E.Z.-C.: eli.zysman-colman@st-andrews.ac.uk.
*E-mail for E.G.M.: egmoore@uq.edu.au.
*E-mail for M.I.O.: m.ogden@curtin.edu.au.
*E-mail for M.M.: m.massi@curtin.edu.au.

ORCID

Massimiliano Massi: 0000-0001-6949-4019

Present Address

[¶]Laboratory of Micro and Submicro Enabling Technologies of the Emilia-Romagna Region S.c.r.l. (MIST E-R S.c.r.l.) via GobeD 101, Bologna 40129, Italy

Notes

The authors declare no competing financial interest.

■ ACKNOWLEDGMENTS

This work was supported by the Australian Research Council and a Royal Society International Exchanges Grant. E.Z.-C. thanks the EPSRC (EP/M02105X/1) for support. L.A.G. and B.L.R. thank Curtin University for a postgraduate scholarship. The authors acknowledge access to the facilities at the Centre for Microscopy, Characterisation and Analysis, University of Western Australia.

■ REFERENCES

(1) Bünzli, J.-C. G. Lanthanide Luminescence for Biomedical Analyses and Imaging. *Chem. Rev.* **2010**, *110* (5), 2729−2755.
(2) Eliseeva, S. V.; Bünzli, J.-C. G. Rare Earths: Jewels for Functional Materials of the Future. *New J. Chem.* **2011**, *35* (6), 1165−1176.
(3) De Bettencourt-Dias, A. Lanthanide-Based Emitting Materials in Light-Emitting Diodes. *Dalton Trans.* **2007**, *49* (22), 2229−2241.
(4) Andres, J.; Hersch, R. D.; Moser, J.-E.; Chauvin, A.-S. A New Anti-Counterfeiting Feature Relying on Invisible Luminescent Full Color Images Printed with Lanthanide-Based Inks. *Adv. Funct. Mater.* **2014**, *24* (32), 5029−5036.
(5) New, E.; Congreve, A.; Parker, D. Definition of the Uptake Mechanism and Sub-Cellular Localisation Profile of Emissive Lanthanide Complexes as Cellular Optical Probes. *Chem. Sci.* **2010**, *1* (1), 111−118.
(6) Butler, S. J.; Delbianco, M.; Lamarque, L.; McMahon, B. K.; Neil, E. R.; Pal, R.; Parker, D.; Walton, J. W.; Zwier, J. M. EuroTracker® Dyes: Design, Synthesis, Structure and Photophysical Properties of Very Bright Europium Complexes and Their Use in Bioassays and Cellular Optical Imaging. *Dalton Trans.* **2015**, *44* (11), 4791−4803.
(7) Bünzli, J. C. G.; Eliseeva, S. V. Photophysics of Lanthanoid Coordination Compounds. In *Comprehensive Inorganic Chemistry II*; Elsevier: Amsterdam, 2013; pp 339−398.
(8) De Bettencourt-Dias, A.; Barber, P. S.; Viswanathan, S. Aromatic N-Donor Ligands as Chelators and Sensitizers of Lanthanide Ion Emission. *Coord. Chem. Rev.* **2014**, *273*−*274*, 165−200.
(9) Moore, E. G.; Samuel, A. P. S.; Raymond, K. N. From Antenna to Assay: Lessons Learned in Lanthanide Luminescence. *Acc. Chem. Res.* **2009**, *42* (4), 542−552.
(10) Binnemans, K. Luminescence of Metallomesogens in the Liquid Crystal State. *J. Mater. Chem.* **2009**, *19* (4), 448−453.
(11) Bünzli, J.-C. G.; Eliseeva, S. V. Basics of Lanthanide Photophysics. In *Lanthanide Luminescence*; Springer: Berlin, Heidelberg, 2010; Springer Series on Fluorescence Vol. 7, pp 1−45.
(12) Andres, J.; Chauvin, A.-S. Energy Transfer in Coumarin-Sensitised Lanthanide Luminescence: Investigation of the Nature of the Sensitiser and Its Distance to the Lanthanide Ion. *Phys. Chem. Chem. Phys.* **2013**, *15* (38), 15981−15994.
(13) Latva, M.; Takalo, H.; Mukkala, V. M.; Matachescu, C.; Rodríguez-Ubis, J. C.; Kankare, J. Correlation Between the Lowest Triplet State Energy Level of the Ligand and Lanthanide (III) Luminescence Quantum Yield. *J. Lumin.* **1997**, *75* (2), 149−169.
(14) Eliseeva, S.; Bünzli, J.-C. G. Lanthanide Luminescence for Functional Materials and Bio-Sciences. *Chem. Soc. Rev.* **2010**, *39* (1), 189−227.
(15) Biju, S.; Gopakumar, N.; Bünzli, J.-C. G.; Scopelliti, R.; Kim, H. K.; Reddy, M. L. P. Brilliant Photoluminescence and Triboluminescence From Ternary Complexes of DyIII and TbIII with 3-Phenyl-4-Propanoyl-5-Isoxazolonate and a Bidentate Phosphine Oxide Coligand. *Inorg. Chem.* **2013**, *52* (15), 8750−8758.
(16) Horrocks, W. D.; Bolender, J. P.; Smith, W. D.; Supkowski, R. M. Photosensitized Near Infrared Luminescence of Ytterbium (III) in Proteins and Complexes Occurs via an Internal Redox Process. *J. Am. Chem. Soc.* **1997**, *119* (25), 5972−5973.
(17) De Bettencourt-Dias, A.; Barber, P. S.; Bauer, S. A Water-Soluble Pybox Derivative and Its Highly Luminescent Lanthanide Ion Complexes. *J. Am. Chem. Soc.* **2012**, *134* (16), 6987−6994.
(18) Glover, P. B.; Bassett, A. P.; Nockemann, P.; Kariuki, B. M.; Van Deun, R.; Pikramenou, Z. Fully Fluorinated Imidodiphosphinate Shells for Visible- and NIR-Emitting Lanthanides: Hitherto Unexpected Effects of Sensitizer Fluorination on Lanthanide Emission Properties. *Chem. - Eur. J.* **2007**, *13* (22), 6308−6320.
(19) Andreiadis, E. S.; Gauthier, N.; Imbert, D.; Demadrille, R.; Pécaut, J.; Mazzanti, M. Lanthanide Complexes Based on β-Diketonates and a Tetradentate Chromophore Highly Luminescent as Powders and in Polymers. *Inorg. Chem.* **2013**, *52* (24), 14382−14390.
(20) Andrews, P. C.; Gee, W. J.; Junk, P. C.; Massi, M. Variation of Structural Motifs in Lanthanoid Hydroxo Clusters by Ligand Modification. *New J. Chem.* **2013**, *37* (1), 35−48.
(21) Wagner, A. T.; Roesky, P. W. Rare-Earth Metal Oxo/Hydroxo Clusters - Synthesis, Structures, and Applications. *Eur. J. Inorg. Chem.* **2016**, *2016* (6), 782−791.
(22) Hou, Y.; Shi, J.; Chu, W.; Sun, Z. Synthesis, Crystal Structure, and Near-IR Luminescent Properties of Lanthanide Bis(β-Diketonate) Complexes. *Eur. J. Inorg. Chem.* **2013**, *2013* (17), 3063−3069.
(23) Biju, S.; Eom, Y. K.; Bünzli, J.-C. G.; Kim, H. K. A New Tetrakis B-Diketone Ligand for NIR Emitting LnIII Ions: Luminescent Doped PMMA Films and Flexible Resins for Advanced Photonic Applications. *J. Mater. Chem. C* **2013**, *1* (42), 6935−6944.
(24) Harrison, B. S.; Foley, T. J.; Bouguettaya, M.; Boncella, J. M.; Reynolds, J. R.; Schanze, K. S.; Shim, J.; Holloway, P. H.; Padmanaban, G.; Ramakrishnan, S. Near-Infrared Electroluminescence From

DOI: 10.1021/acs.inorgchem.7b00928
Inorg. Chem. 2017, 56, 8975−8985

Conjugated Polymer/Lanthanide Porphyrin Blends. *Appl. Phys. Lett.* **2001**, *79* (23), 3770−3372.
(25) Reddy, M. L. P.; Divya, V.; Pavithran, R. Visible-Light Sensitized Luminescent Europium(III)-β-Diketonate Complexes: Bioprobes for Cellular Imaging. *Dalton Trans.* **2013**, *42* (43), 15249−15262.
(26) Crosby, G. A.; Whan, R. E.; Alire, R. M. Intramolecular Energy Transfer in Rare Earth Chelates. Role of the Triplet State. *J. Chem. Phys.* **1961**, *34* (3), 743−748.
(27) Crosby, G. A.; Whan, R. E. Extreme Variations of the Emission Spectra of Dysprosium Chelates. *J. Chem. Phys.* **1960**, *32* (2), 614−615.
(28) Ismail, M.; Lyle, S. J.; Newbery, J. E. Some Lanthanide and Group II Complexes with Triketones. *J. Inorg. Nucl. Chem.* **1969**, *31* (7), 2091−2093.
(29) Reid, B. L.; Stagni, S.; Malicka, J. M.; Cocchi, M.; Sobolev, A. N.; Skelton, B. W.; Moore, E. G.; Hanan, G. S.; Ogden, M. I.; Massi, M. Lanthanoid/Alkali Metal β-Triketonate Assemblies: a Robust Platform for Efficient NIR Emitters. *Chem. - Eur. J.* **2015**, *21*, 18354−18363.
(30) Bünzli, J.-C. G. On the Design of Highly Luminescent Lanthanide Complexes. *Coord. Chem. Rev.* **2015**, *293*−*294*, 19−47.
(31) Reid, B. L.; Stagni, S.; Malicka, J. M.; Cocchi, M.; Hanan, G. S.; Ogden, M. I.; Massi, M. Lanthanoid β-Triketonates: a New Class of Highly Efficient NIR Emitters for Bright NIR-OLEDs. *Chem. Commun.* **2014**, *50* (78), 11580−11582.
(32) Thielemann, D. T.; Klinger, M.; Wolf, T. J. A.; Lan, Y.; Wernsdorfer, W.; Busse, M.; Roesky, P. W.; Unterreiner, A.-N.; Powell, A. K.; Junk, P. C.; Deacon, G. B. Novel Lanthanide-Based Polymeric Chains and Corresponding Ultrafast Dynamics in Solution. *Inorg. Chem.* **2011**, *50* (23), 11990−12000.
(33) Cametti, M.; Nissinen, M.; Dalla Cort, A.; Mandolini, L.; Rissanen, K. Recognition of Alkali Metal Halide Contact Ion Pairs by Uranyl−Salophen Receptors Bearing Aromatic Sidearms. the Role of Cation−Π Interactions. *J. Am. Chem. Soc.* **2005**, *127* (11), 3831−3837.
(34) Mahadevi, A. S.; Sastry, G. N. Cation−Π Interaction: Its Role and Relevance in Chemistry, Biology, and Material Science. *Chem. Rev.* **2013**, *113* (3), 2100−2138.
(35) Andreiadis, E. S.; Imbert, D.; Pécaut, J.; Demadrille, R.; Mazzanti, M. Self-Assembly of Highly Luminescent Lanthanide Complexes Promoted by Pyridine-Tetrazolate Ligands. *Dalton Trans.* **2012**, *41* (4), 1268−1277.
(36) Mehlstäubl, M.; Kottas, G. S.; Colella, S.; De Cola, L. Sensitized Near-Infrared Emission From Ytterbium(III) via Direct Energy Transfer From Iridium(III) in a Heterometallic Neutral Complex. *Dalton Trans.* **2008**, *102* (18), 2385−2388.
(37) Binnemans, K. Interpretation of Europium(III) Spectra. *Coord. Chem. Rev.* **2015**, *295*, 1−45.
(38) Casanova, D.; Llunell, M.; Alemany, P.; Alvarez, S. The Rich Stereochemistry of Eight-Vertex Polyhedra: a Continuous Shape Measures Study. *Chem. - Eur. J.* **2005**, *11* (5), 1479−1494.
(39) Martín-Ramos, P.; Silva, M. R.; Lahoz, F.; Martín, I. R.; Chamorro-Posada, P.; Eusebio, M. E. S.; Lavín, V.; Martín-Gil, J. Journal of Photochemistry and Photobiology a: Chemistry. *J. Photochem. Photobiol., A* **2014**, *292*, 16−25.
(40) Tan, R. H. C.; Motevalli, M.; Abrahams, I.; Wyatt, P. B.; Gillin, W. P. Quenching of IR Luminescence of Erbium, Neodymium, and Ytterbium β-Diketonate Complexes by Ligand C−H and C−D Bonds. *J. Phys. Chem. B* **2006**, *110* (48), 24476−24479.
(41) Shavaleev, N. M.; Scopelliti, R.; Gumy, F.; Bünzli, J.-C. G. Modulating the Near-Infrared Luminescence of Neodymium and Ytterbium Complexes with Tridentate Ligands Based on Benzoxazole-Substituted 8-Hydroxyquinolines. *Inorg. Chem.* **2009**, *48* (7), 2908−2918.
(42) Shavaleev, N. M.; Scopelliti, R.; Gumy, F.; Bünzli, J.-C. G. Surprisingly Bright Near-Infrared Luminescence and Short Radiative Lifetimes of Ytterbium in Hetero-Binuclear Yb−Na Chelates. *Inorg. Chem.* **2009**, *48* (16), 7937−7946.
(43) Martín-Ramos, P.; Pereira da Silva, P. S.; Lavín, V.; Martín, I. R.; Lahoz, F.; Chamorro-Posada, P.; Ramos Silva, M.; Martín-Gil, J. Structure and NIR-Luminescence of Ytterbium(III) Beta-Diketonate Complexes with 5-Nitro-1,10-Phenanthroline Ancillary Ligand: Assessment of Chain Length and Fluorination Impact. *Dalton Trans.* **2013**, *42* (37), 13516−13526.
(44) Poisson, L.; Roubin, P.; Coussan, S.; Soep, B.; Mestdagh, J.-M. Ultrafast Dynamics of Acetylacetone (2,4-Pentanedione) in the S2 State. *J. Am. Chem. Soc.* **2008**, *130* (10), 2974−2983.
(45) Reid, B. L.; Moore, E. G.; Skelton, B. W.; Ogden, M. I.; Massi, M. Investigation of the Photophysical Properties of a Eu^{3+} Coordination Polymer Bearing an α-Nitrile Substituted β-Diketonate Ligand via Emission and Ultrafast Transient Absorption Spectroscopy. *Aust. J. Chem.* **2015**, *68* (9), 1392−1398.
(46) Verma, P. K.; Steinbacher, A.; Koch, F.; Nuernberger, P.; Brixner, T. Monitoring Ultrafast Intramolecular Proton Transfer Processes in an Unsymmetric β-Diketone. *Phys. Chem. Chem. Phys.* **2015**, *17* (13), 8459−8466.
(47) Paris, C.; Lhiaubet-Vallet, V.; Jiménez, O.; Trullas, C.; Miranda, M. Á. A Blocked Diketo Form of Avobenzone: Photostability, Photosensitizing Properties and Triplet Quenching by a Triazine-Derived UVB-Filter. *Photochem. Photobiol.* **2009**, *85* (1), 178−184.
(48) de Mello, J. C.; Wittmann, H. F.; Friend, R. H. An Improved Experimental Determination of External Photoluminescence Quantum Efficiency. *Adv. Mater.* **1997**, *9* (3), 230−232.
(49) Zawadiak, J.; Mrzyczek, M. Influence of Substituent on UV Absorption and Keto−Enol Tautomerism Equilibrium of Dibenzoylmethane Derivatives. *Spectrochim. Acta, Part A* **2012**, *96*, 815−819.
(50) Sheldrick, G. M. Crystal Structure Refinement with SHELXL. *Acta Crystallogr., Sect. C: Struct. Chem.* **2015**, *71* (1), 3−8.

DOI: 10.1021/acs.inorgchem.7b00928
Inorg. Chem. 2017, 56, 8975−8985